UNCERTAINTY QUANTIFICATION IN AEROELASTIC RESPONSE OF AN IDEALIZED COMPOSITE WING

Christian T. Nitschke[1], Jonas Maruani[1], Angela Vincenti[1], Didier Lucor[1], and Jean-Camille Chassaing[1]

[1]Sorbonne Universités, UPMC Univ Paris 06, CNRS, UMR 7190, Institut Jean Le Rond d'Alembert
4 Place Jussieu, 75252 Paris Cedex 05, France
christian.nitschke@upmc.fr

Keywords: aeroelasticity, composite materials, arbitrary polynomial chaos, polar method

Abstract: The aeroelastic response of a cantilevered composite plate wing in incompressible flow is studied. Uncertainties of the laminate ply angles are taken into account, with special regard to desymmetrisation of the laminate by the uncertainties. The polar method is employed for preliminary analysis as well as parameter space reduction. Arbitrary polynomial chaos is used to decrease the number of calls to the aeroelastic solver.

1 INTRODUCTION

In aeroelastic design of aircraft structures, composite materials are employed more and more often in order to increase their performance and to reduce their weight. These materials suffer from a great number of uncertainties from various sources [1]. Studies showed that these uncertainties affect the aeroelastic properties [2].

While there are possibilities to obtain stochastic properties from measurements on entire composite layups [3, 4], a key uncertainty remains the error in the ply angles [5]. Scarth and Cooper [6] achieved a significant breakthrough in estimating the aeroelastic response to layup errors in symmetric laminates using lamination parameters.

In the present work, this research is extended to laminates of which the plies are desymmetrized by the uncertainty in the layup angles. The polar method [7] is used to perform a preliminary analysis of the composite material. Then, the uncertain material parameters are propagated to obtain the aeroelastic response of a plate wing in incompressible flow, using a Rayleigh- Ritz structural model combined with quasi-steady aerodynamics [8–10]. To reduce the number of calls to the aeroelastic solver, a polynomial chaos approach is employed, taking advantage of the reduction of the number of uncertain parameters by the polar method. As the polar parameters are correlated, we use a Gram-Schmidt orthogonalization to construct the necessary polynomial basis [11, 12].

2 AEROELASTIC MODEL

We consider a cantilevered composite rectangular plate wing, of which the instability behaviour is computed using the Rayleigh-Ritz method. A scheme of the studied configuration can be found in Fig. (1)

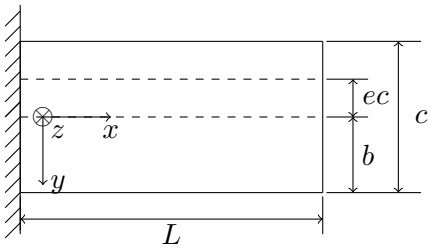

Figure 1: Scheme of the studied cantilevered plate wing configuration

The Rayleigh-Ritz method is derived from the expressions for the potential and kinetic energy. We neglect in-plane forces in this case and only take into account out-of-plane bending and loads. The potential energy of a plate is given in that case as [6]

$$U = \frac{1}{2}\int_{-b}^{b}\int_{0}^{L} \kappa^T \tilde{\mathbf{D}} \kappa dx dy \tag{1}$$

with the tensor of curvatures

$$\kappa = \begin{Bmatrix} -\frac{\partial^2 h}{\partial x^2} \\ -\frac{\partial^2 h}{\partial y^2} \\ -2\frac{\partial^2 h}{\partial x \partial y} \end{Bmatrix} \tag{2}$$

$\tilde{\mathbf{D}}$ the bending stiffness matrix, b the half chord and L the half span.

The kinetic energy of the plate is given as

$$T = -\frac{1}{2}\rho d \int_{-b}^{b}\int_{0}^{L} \left(\frac{\partial h}{\partial t}\right)^2 dx dy \tag{3}$$

where d is the total thickness of the laminated plate.

Following a Rayleigh-Ritz approach, the out-of-plane displacement can be written as [8]

$$h(x,y,t) = \sum_{i=1}^{N_{modes_x}} \sum_{j=1}^{N_{modes_y}} \phi_i(x)\psi_j(y)\hat{h}_{ij}(t) \tag{4}$$

We will use the form functions for a clamped-free [CFFF] plate proposed by [8]

$$\phi_i(x) = \left(\frac{x}{L}\right)^{i+1}, \psi_j(y) = \left(\frac{y}{c}\right)^{j-1} \tag{5}$$

These function definition is substituted into equations (1) and (3) expressions are inserted into the Lagrangian equations

$$\frac{d}{dt}\frac{\partial T}{\partial \dot{\hat{h}}_{ij}} - \frac{\partial T}{\partial \hat{h}_{ij}} + \frac{\partial U}{\partial \hat{h}_{ij}} = \frac{\partial(\delta W)}{\partial(\delta \hat{h}_{ij})} \tag{6}$$

The virtual work is contributed by the aerodynamic lift and moment forces. For computing them, we use the quasi-steady aerodynamic operator from [9], who give the lift and moment terms for an infinitesimal wing section as

$$dL = \frac{1}{2}\rho_a U^2 c a_w \left(\frac{\dot{h}}{U} + \theta\right) dx \tag{7}$$

$$dM = \frac{1}{2}\rho_a U^2 c^2 \left[e a_w \left(\frac{\dot{h}}{U}\right) + M_{\dot{\theta}} \left(\frac{\dot{\theta} c}{4U}\right)\right] dx \tag{8}$$

where U is the airspeed, ρ_a is the air density and c is the chord. $a_w = 2\pi\left[1 - \left(\frac{x}{L}\right)\right]$ is a term to include wing tip effects. e is the nondimensional distance between the reference axis, which is set to midchord here, and the point of attack of the lift and moment. This is 0.25 for strip theory aerodynamics on flat plates. $M_{\dot{\theta}}$ is a term to include unsteady effects in the flow with respect to the angular movement of the wing. [9] set it to $M_{\dot{\theta}} = -1.2$, which we also do.

Note that the fact that this model does not account for camber, but is done for a flat plate segment. This means we have to limit $N_{modes_y} \leq 2$. The deflection angle θ can be deduced from Eq. (4) via a small deflection and small angle hypothesis.

The equations can be written in matrix form as general eigenvalue problem [10]

$$\begin{pmatrix} \mathbf{I} & \mathbf{0} \\ \mathbf{0} & \mathbf{A} \end{pmatrix} \dot{\hat{\mathbf{h}}} = \begin{pmatrix} \mathbf{0} & \mathbf{I} \\ -(-\mathbf{C}+\mathbf{E}) & \mathbf{B} \end{pmatrix} \hat{\mathbf{h}} \tag{9}$$

where $\mathbf{I}$ is the identity matrix, $\mathbf{A}$ the structural inertia matrix, $\mathbf{B}$ the aerodynamic damping matrix, $\mathbf{C}$ the aerodynamic stiffness matrix and $\mathbf{E}$ the structural stiffness matrix.

The system becomes unstable when the real part of the eigenvalues becomes positive, where the behaviour is flutter when the imaginary part of the eigenvalues is non-zero.

3 THE POLAR METHOD

To obtain the polar constants, the tensor is transformed by a complex base change [13]. Afterwards, the polar components can easily computed as invariants. When this method is applied to the plane stiffness tensor $\mathbf{Q}$ for any anisotropic material layer, the polar decomposition is described as follows [14]

$$8T_0 = Q_{xx} - 2Q_{xy} + 4Q_{ss} + Q_{yy} \tag{10}$$

$$8T_1 = Q_{xx} + 2Q_{xy} + Q_{yy} \tag{11}$$

$$8R_0 e^{\imath 4\Phi_0} = Q_{xx} + 4\imath Q_{xs} - 2Q_{xy} - 4Q_{ss} - 4\imath Q_{ys} + Q_{yy} \tag{12}$$

$$8R_1 e^{\imath 2\Phi_1} = Q_{xx} + 2\imath Q_{xs} + 2\imath Q_{ys} - Q_{yy} \tag{13}$$

T_0 and T_1 represent the isotropic part of the stiffness, whereas R_0 and R_1 represent the anisotropic behaviour. Φ_0 and Φ_1 denote the angles of the deviation of the material behaviour with respect

to the reference axis. Quantities T_0, T_1, R_0, R_1 and $(\Phi_0 - \Phi_1)$ are invariants, whilst angles Φ_0 and Φ_1 depend on the choice of the reference frame.

The cartesian representation of the stiffness tensor can be obtained from the polar constants as [14]

$$
\begin{aligned}
Q_{xx} &= T_0 + 2T_1 + R_0\cos(4\Phi_0) + 4R_1\cos(2\Phi_1) && (14)\\
Q_{xy} &= -T_0 + 2T_1 - R_0\cos(4\Phi_0) && (15)\\
Q_{xs} &= R_0\sin(4\Phi_0) + 2R_1\sin(2\Phi_1) && (16)\\
Q_{yy} &= T_0 + 2T_1 + R_0\cos(4\Phi_0) - 4R_1\cos(2\Phi_1) && (17)\\
Q_{ys} &= -R_0\sin(4\Phi_0) + 2R_1\sin(2\Phi_1) && (18)\\
Q_{ss} &= T_0 - R_0\cos(4\Phi_0) && (19)
\end{aligned}
$$

Elastic symmetry	Polar condition
Orthotropy	$\Phi_0 - \Phi_1 = K\frac{\pi}{4}$
R_0-Orthotropy	$R_0 = 0$
Square Symmetry	$R_1 = 0$
Isotropy	$R_0 = R_1 = 0$

Table 1: Conditions for elastic symmetries in terms of polar invariants [13]

As we are interested in the coupled bending behaviour of a composite plate, we will apply this mechanism on the classical laminated plate theory. The lineic forces $\mathbf{N}$ and moments $\mathbf{M}$ are linked to the lineic mid-plane strains ε_0 and curvatures κ by the following matrix

$$
\begin{pmatrix} \mathbf{N} \\ \mathbf{M} \end{pmatrix} = \begin{pmatrix} \mathbf{A} & \mathbf{B} \\ \mathbf{B} & \mathbf{D} \end{pmatrix} \begin{pmatrix} \varepsilon_0 \\ \kappa \end{pmatrix} \tag{20}
$$

where $\mathbf{A}$ is the membrane stiffness, $\mathbf{D}$ the bending stiffness and $\mathbf{B}$ describes the coupling between the membrane and the bending forces.

In the case considered, the plate is not subject to in-plane membrane forces ($\mathbf{N} = \mathbf{O}$). However, the membrane stiffnesses contribute to the bending behaviour. This can be described by a modified bending stiffness tensor

$$
\tilde{\mathbf{D}} = \mathbf{D} - \mathbf{B}\mathbf{A}^{-1}\mathbf{B} \tag{21}
$$

The polar formalism will be applied to this modified bending stiffness tensor, thus its polar components are $\tilde{T}_0, \tilde{T}_1, \tilde{R}_0, \tilde{R}_1, \tilde{\Phi}_0, \tilde{\Phi}_1$, according to relations Eq. (10 - 13).

4 STOCHASTIC FRAMEWORK

Polynomial chaos approaches have long been used to reduce the computational cost of non-intrusive stochastic analysis compared to the standard Monte Carlo method. However, the classical decompositions are limited to uncorrelated variables of a small number of distribution families. Especially in the case of strong correlation, this makes it necessary to either decompose the domain [15] or to decorrelate the input variables, for example by Karhunen-Loève

decomposition [16] or Rosenblatt transformations [6]. However, these approaches require either certain types of correlation or knowledge of the analytical form of the joint posterior CDF, which may be tedious to compute.

In 2004, Soize presented a generalised method to derive the needed orthogonal polynomial basis for polynomial chaos expansions [11]. Recently, it was shown that this approach can be used with correlated input variables [12]. We will adopt this scheme in the following.

The random variables considered for the present analysis are the polar components of the bending tensor $\tilde{\mathbf{D}}$

$$\theta = \{\tilde{T}_0, \tilde{T}_1, \tilde{R}_0, \tilde{R}_1, \tilde{\Phi}_0, \tilde{\Phi}_1\} \tag{22}$$

which gives us $N = 6$ random variables. Response surfaces will be generated from an orthogonal polynomial basis of order P. Orthogonality is defined in the sense of a polynomial scalar product

$$\int_\Theta \phi_i(\theta)\phi_j(\theta)p(\theta)d\theta = \mathbb{E}\{\phi_i(\theta)^2\}\delta_{ij} \tag{23}$$

The M generated polynomials will then be used in the polynomial chaos representation

$$u(\theta) = \sum_{i=1}^{M} \hat{u}_i \phi_i(\theta) \tag{24}$$

The polynomial basis is generated using a Gram-Schmidt orthogonalisation process as follows [12]

$$\phi_0(\theta) = 1 \tag{25}$$

$$\phi_j(\theta) = e_j(\theta) - \sum_{k=0}^{j-1} c_{jk}\phi_k(\theta) \tag{26}$$

where $e_j = \{1, \theta_1, \theta_2, \ldots, \theta_6, \theta_1^2, \theta_1\theta_2, \theta_1\theta_3, \ldots\}$ and the coefficients c_{jk} are computed as

$$c_{jk} = \frac{\langle e_j(\theta), \phi_k(\theta)\rangle}{\langle \phi_k(\theta), \phi_k(\theta)\rangle} \tag{27}$$

$\langle \cdot, \cdot \rangle$ denotes a polynomial scalar product as defined in Eq. (23). The necessary integrals are computed using Monte Carlo integration.

The expansion coefficients are fitted using least squares regression on a random set of points in six-dimensional space.

The procedure has been validated against the test case of [12], where analytical solutions for an example problem are given. Moreover, for a certain choice of parameters, the input becomes uncorrelated, which enables further validation of the algorithm in comparison to classical Hermite polynomial chaos. This comparison is shown in Fig. (2)

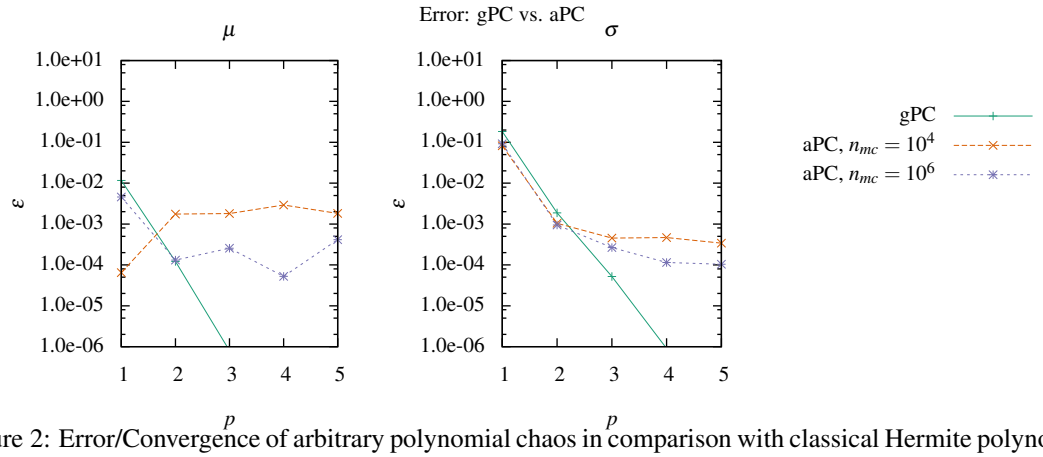

Figure 2: Error/Convergence of arbitrary polynomial chaos in comparison with classical Hermite polynomial chaos as a function of the polynomial order. Test case from [12]

5 COMPOSITE BEHAVIOUR

The use of anisotropic materials means that in addition to aerodynamic coupling of the modes, elastic mode coupling is to be expected. To be capable of interpreting the elastic contribution to mode coupling, we examine the bending stiffness behaviour using the polar method.

For reasons of comparability, we will rely on the base material used by [6], which is an orthotropic layer made of unidirectional carbon fibres in an epoxy matrix. The elastic properties are given in Tab. (2). The corresponding polar constants are given in Tab. (3).

$E_1[GPa]$	$E_2[GPa]$	$G_{12}[GPa]$	ν_{12}	$t[mm]$
140	10	5	0.3	0.125

Table 2: Elastic moduli of base material [6]

$T_0[GPa]$	$T_1[GPa]$	$R_0[GPa]$	$R_1[GPa]$	$\Phi_0[^\circ]$	$\Phi_1[^\circ]$
20.62	19.63	15.62	16.36	0.0	0.0

Table 3: Polar components of elastic behaviour of base material in Tab. (2)

From this base layer, layups are constructed, which again are chosen from [6]. They are given in Tab. (4), along with the deterministic polar constants for the modified bending stiffness.

These stacking sequences are composed by 16 layers in symmetric configuration. They are thus nominally uncoupled ($\mathbf{B} = \mathbf{O}$). In this case, $\tilde{\mathbf{D}} = \mathbf{D}$ (see Eq. (21)). From this table, we see that for the nominal symmetric laminates, the isotropic components of the material behaviour do not depend on the layup, whereas the anisotropic components change. Despite the regular layup (i.e. angle-ply or quasi-isotropic orientations) of the laminates h) to j), the nominal bending behaviour is not orthotropic, with considerable directional behaviour. this can also be seen observing $\sin(4\Phi_0 - \Phi_1)$, which can be considered as a measure of deviation from orthotropy. Note that materials h) and i) have very similar behaviour except of the polar angles.

Next, we will introduce uncertainties to the angles of the laminate plies. As in [6], the nominal ply angles are used as mean and the standard deviation is set to five degrees. In contrast to the lamination parameter method presented there, the polar method does not require the laminate to

	Layup	$\tilde{T}_0[Nm]$	$\tilde{T}_1[Nm]$	$\tilde{R}_0[Nm]$	$\tilde{R}_1[Nm]$	$\tilde{\Phi}_0[^\circ]$	$\tilde{\Phi}_1[^\circ]$	$\sin 4(\Phi_0-\Phi_1)$
b)	$[(30_2,-30_2)_2]_S$	13.744	13.084	6.207	6.501	36.749	16.502	0.988
h)	$[0_2,90_2,45_2,-45_2]_S$	13.744	13.084	7.808	3.232	0.0	9.217	−0.6
i)	$[45_2,-45_2,0_2,90_2]_S$	13.744	13.084	7.808	3.232	45.0	35.783	0.6
j)	$[90_2,45_2,-45_2,0_2]_S$	13.744	13.084	1.9521	6.465	0.0	80.783	0.6

Table 4: Polar components of nominal bending stiffness for the test laminates with base layer from Tab. (2).

be symmetric to have the number of uncertain parameters reduced to six. Therefore, we allow the angular uncertainties to desymmetrise the laminate, so $N = 16$ independent uncertainties on the angles are considered. This is compared with a laminate where the ply angles are kept symmetric artificially.

We first show the results for laminate b), which is designed to have stronger directional behaviour than the other example laminates. Gaussian kernel density estimations of the uncertainty propagation are given in Fig. (3).

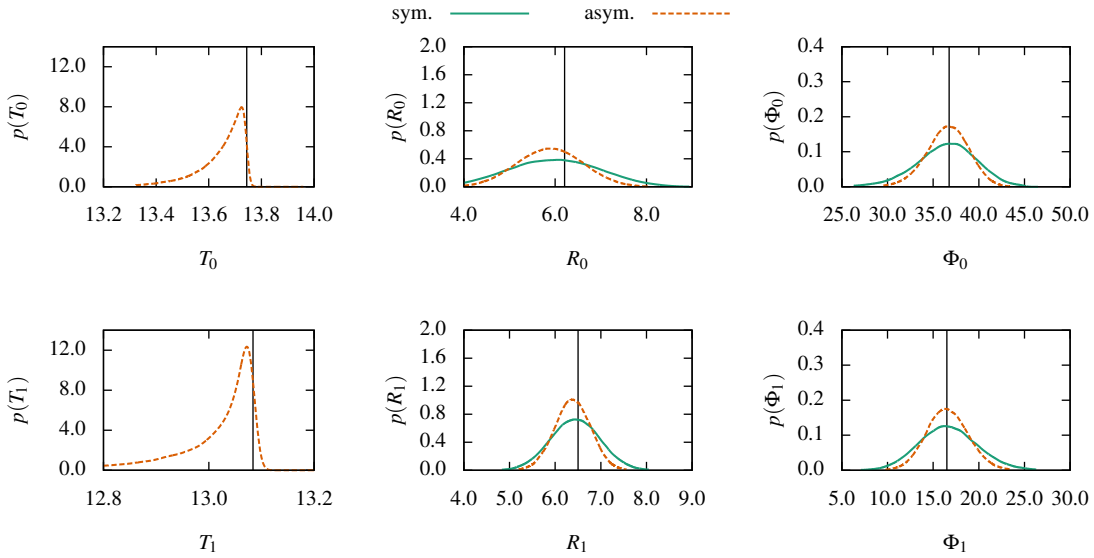

Figure 3: Estimated probability density distribution of polar constants for material b) from Tab. (4) for symmetric laminate and laminate desymmetrized by uncertainty. The vertical line shows the nominal deterministic values.

As expected, the directional behaviour of the laminate is subject to high variation. The properties are well distributed around their nominal value.

The isotropic material properties remain constant in the case of a symmetrised laminate. When the symmetry of the laminate is destroyed, they become also uncertain. The range of variation is, however, still much smaller than that of the anisotropic/coupled stiffnesses. We explain this with membrane/bending coupling setting in, furnishing stiffness against more complex movements at the expense of stiffness against modes including only bending and torsion.

In this context, it is surprising that the range of variation of the polar parameters for coupling is reduced when removing the symmetry constraint. This could be explained by compensation of the random angles, where in the symmetric case, the spread of stiffness would be increased because the plies have to move in the same direction.

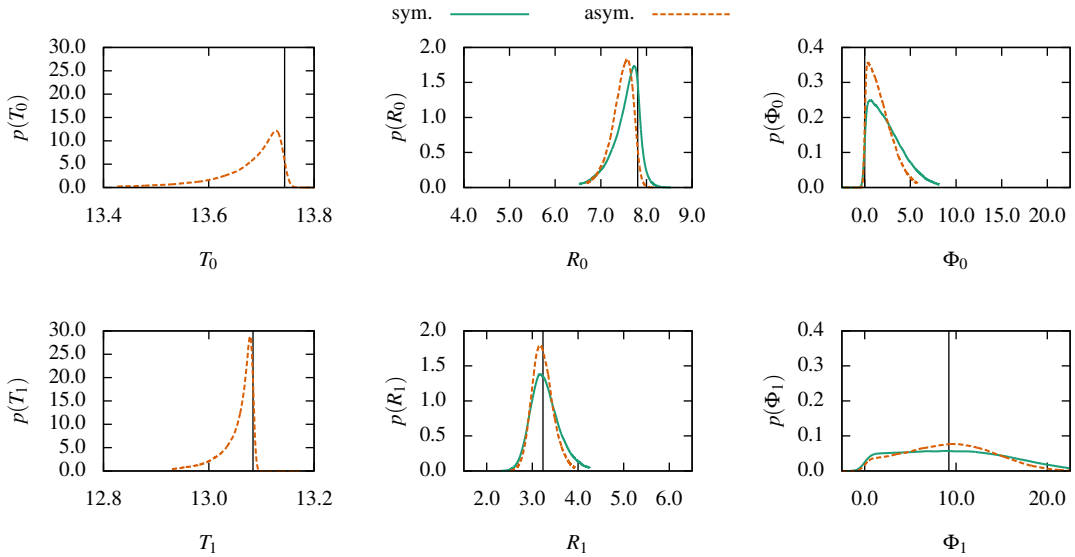

Figure 4: Estimated probability density distribution of polar constants for material h) from Tab. (4) for symmetric laminate and laminate desymmetrized by uncertainty

For the laminate h), of which the polar property distributions are shown in Fig. (4), the spread in the material behaviour is much smaller, which can be attributed to the more regular layup. In contrast to laminate b), the distributions are less symmetric around the nominal bending stiffness values. R_0 is likely to decrease, whereas R_1 has a tendency to increase. [6] show a risk for instability mechanism switches for similar kinds of laminates. The difference found in the anisotropic parameters could be an explanation for that. The cut in the distribution of the angles comes from their definition range.

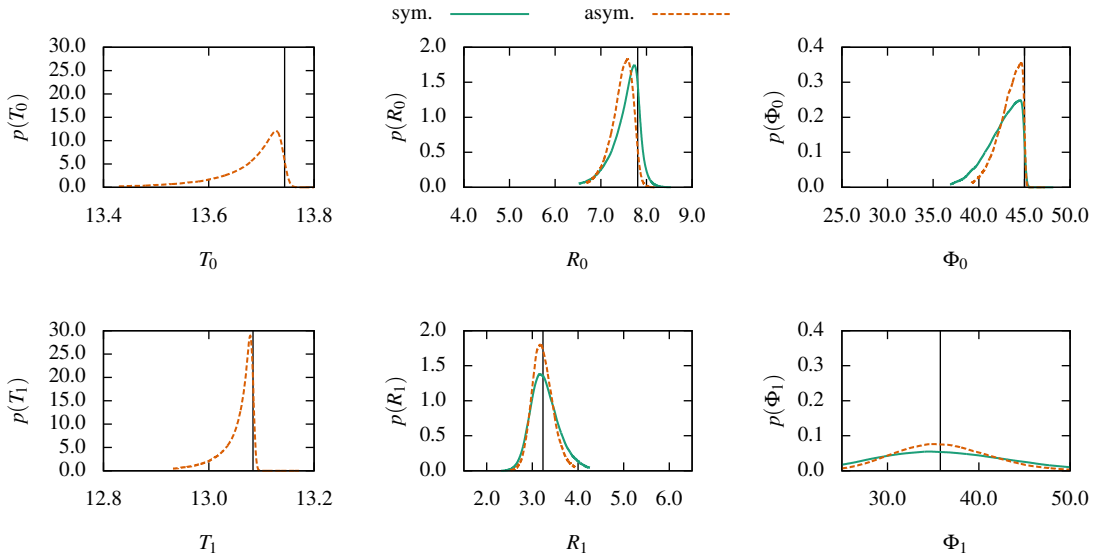

Figure 5: Estimated probability density distribution of polar constants for material i) from Tab. (4) for symmetric laminate and laminate desymmetrized by uncertainty

Laminate i), of which the uncertain properties are shown in Fig. (5) behaves similarly to laminate h) shown in Fig. (5). The most notable difference is found in the polar angles, where coefficient Φ_0 tends to 45 degrees instead of 0. However, the difference between Φ_0 and Φ_1 is identical.

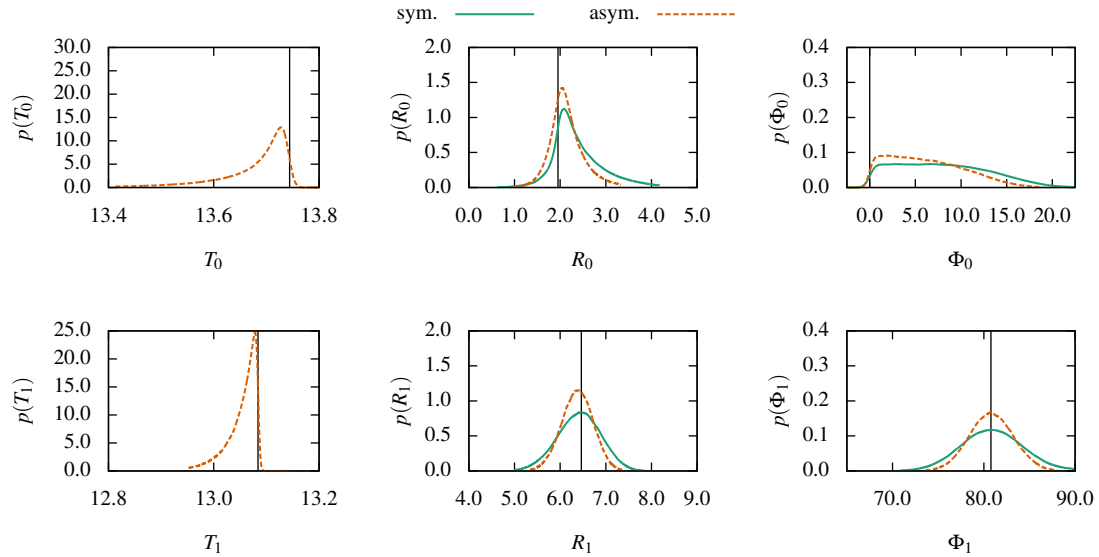

Figure 6: Estimated probability density distribution of polar constants for material j) from Tab. (4) for symmetric laminate and laminate desymmetrized by uncertainty

Laminate j) has a similar structure as laminates h) and i), however, its polar constants reveal quite different properties, as stated in Tab. (4). This also shows in the uncertain behaviour, where the laminate exhibits a much higher spread in anisotropic properties. R_0 has a tendency to increase in this case, whereas R_1 is distributed quite symmetrically around the nominal value. The angular spread in Φ_0 has a particularly high range of variation.

In order to illustrate the dependencies between the stochastic polar parameters, we plot in Fig. (7) the scatter plots for laminate b).

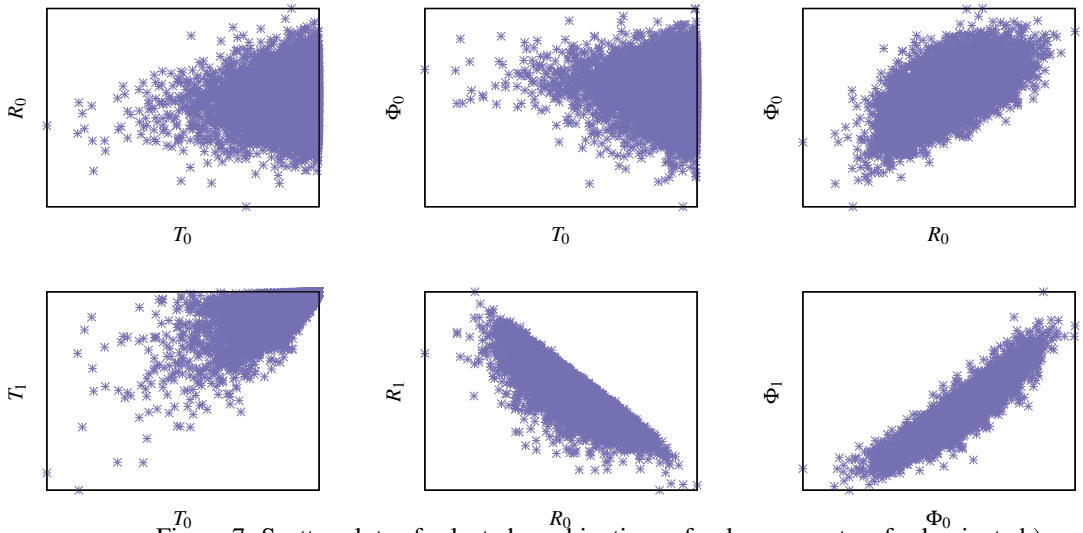

Figure 7: Scatter plots of selected combinations of polar parameters for laminate b)

The upper line shows an example of correlations of the polar parameters linked to the same tensor part. The line below shows the correlations between polar parameters of the same type for the different tensor parts. It is shown that the correlations between the polar parameters is linked to the definition range, which itself depends on the material symmetry. Except for the isotropic constants, the correlations between anisotropic constants of the same type are almost linear.

In conclusion, it has been shown that the uncertain material behaviour, especially with regard to the spread of the anisotropic/coupled bending stiffnesses, depends very much on the chosen layup strategy. Directional layups suffer more from the uncertainty than balanced ones. As this kind of strategies is used heavily in aeroelastic design/tailoring to influence aeroelastic coupling, we expect this to affect the results for the flutter velocity.

6 FLUTTER RESULTS

Now, the uncertain stiffnesses from the previous section are propagated through the model presented in Section 2. The aeromechanical parameters are given in Tab. (5).

$\rho\,[kg/m^3]$	$c[m]$	$L[m]$	$\rho_a\,[kg/m^3]$	$M_{\dot{\theta}}$	e
1600	0.0762	0.3048	1.2574	-1.2	0.25

Table 5: Aeromechanical parameters used for computation of the flutter speed

Contrary to [6], only the flutter phenomenon is examined; thus, this study does not account for divergence. The results for the four test laminates are shown in Fig. (8).

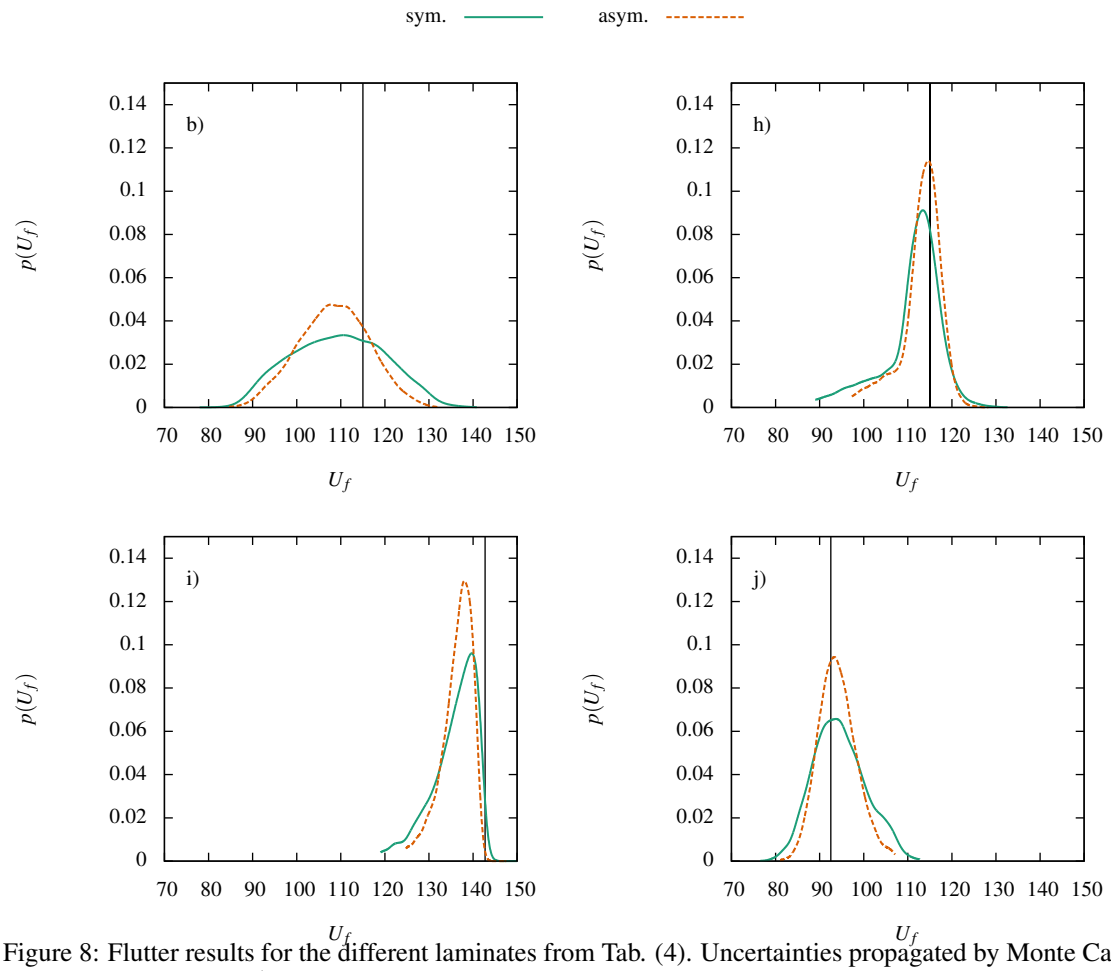

Figure 8: Flutter results for the different laminates from Tab. (4). Uncertainties propagated by Monte Carlo Simulation with 10^4 samples.

As could be expected from the study of the polar parameters, plate wings constructed from laminates with higher directionality are more prone to uncertainties in the ply angles. Therefore,

laminate b) exhibits the highest standard deviation in flutter velocity.

Changes in anisotropic bending stiffness have direct impact on the flutter speed. Most of the uncertainty can directly be attributed to this effect. In cases where the uncertainty leads to reduced mean anisotropic bending stiffness, as is the case for laminates h) and i), it is notable that the mean flutter speed also has a tendency to decrease. In contrast, when the mean of the anisotropic constants has a tendency to increase, the flutter speed also follows.

These tendencies are kept when the laminate symmetry is destroyed by the uncertainty in the ply angles. However, the standard deviation of the flutter speed also follows the standard deviation of the anisotropic constants and decreases.

The Monte Carlo simulation method used up to this point needs many calls to the aeroelastic solver. For this case, these calls are cheap, but for more advanced models, a reduction in the number of calls for the solver is desirable. We apply thus the surrogate model approach presented in Section 4. The surrogate metamodel is constructed using 10000 samples of the polar parameters for integration of the polynomials during the Gram-Schmidt orthogonalization. This does not require any calls of the solver, so this step is computationally cheap. We use then 1000 Monte Carlo samples of U_f obtained through the aeroelastic solver to fit the expansion coefficients of the aPC models by ordinary least squares. As the solver is called, this step can have a considerable cost in computation time. Finally, the aPC model is sampled to obtain an estimation of the final probability density function.

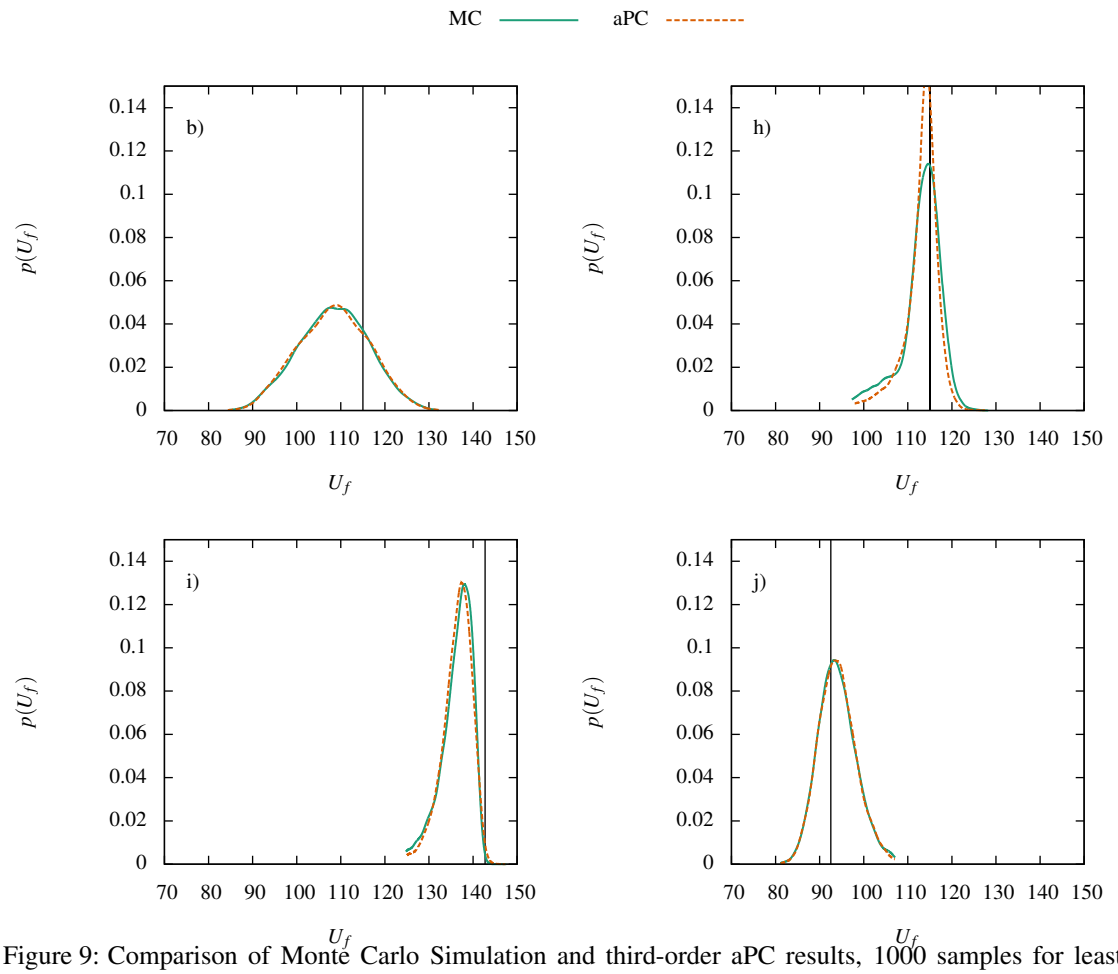

Figure 9: Comparison of Monte Carlo Simulation and third-order aPC results, 1000 samples for least squares fitting of the response surface. Results are shown for desymmetrized laminates.

The comparison shown between Monte Carlo simulation and the arbitrary polynomial chaos in Fig. (9) shows a good agreement for laminates b), i) and j). Only for laminate h), we see that the probability distribution function is estimated too pointed. During tests, it was observed that the convergence of the method for given polynomial order is mainly driven by two limiting factors. First, there is the number of Monte Carlo samples used for the Gram-Schmidt orthogonalisation. The noise of the Monte Carlo integration puts a "floor" to the precision that can be obtained. Once this floor is reached, increasing the polynomial order further does not lead to a decrease in error. Second, there is the number of samples used for the fitting of the expansion coefficients. We found this number to be highly problem-dependent. The number of 1000 samples is a worst-case scenario, some examples being reliably converged at 100 samples.

7 CONCLUSION

In this work, we studied the flutter behaviour of a cantilevered composite plate wing. The effect of uncertainties in the ply angles were examined. We considered symmetric laminates as well as laminates desymmetrised by the aforementioned uncertainties. We first analysed the composite behaviour using the polar method, revealing important variations in anisotropic properties. With the symmetry of the laminate destroyed, we also found variations in the isotropic properties, whereas the standard deviation of the anisotropic properties decreased. The results allowed direct conclusions regarding the flutter speed. Most notably, the critical flutter velocity was

found to be strongly linked to the anisotropic behaviour. The decrease in standard deviation of the anisotropic bending stiffnesses was also found in the flutter response.

A side effect of the use of the polar method is the reduction of dimensionality, which allowed for the use of a polynomial chaos model to reduce the number of calls to the solver. To deal with the correlation of the polar parameters, Gram-Schmidt orthogonalisation was employed in order to construct the polynomial basis. To determine the expansion coefficients, least squares regression was used. Despite the number of parameters is quite high, results show good agreement with a Monte Carlo simulation. In comparison with the latter, the arbitrary polynomial chaos method allowed to reduce the number of calls to the deterministic solver by at least a factor of ten.

Further work will include studies on instability mechanism switching, as well as further improvements of the aPC surrogate model, including precision upgrades, reduction of the number of calls to the solver and partitioning of the parameter space.

8 REFERENCES

[1] Sriramula, S. and Chryssanthopoulos, M. K. (2009). Quantification of uncertainty modelling in stochastic analysis of FRP composites. *Composites Part A: Applied Science and Manufacturing*, 40(11), 1673–1684. ISSN 1359835X. doi: 10.1016/j.compositesa.2009.08.020.

[2] Ouyang, Q., Chen, X., and Cooper, J. E. (2013). Robust Aeroelastic Analysis and Optimization of Composite Wing Under μ-Analysis Framework. *Journal of Aircraft*, 50(4), 1299–1305. ISSN 0021-8669, 1533-3868. doi:10.2514/1.C031915.

[3] Gogu, C., Yin, W., Haftka, R., et al. (2013). Bayesian Identification of Elastic Constants in Multi-Directional Laminate from Moiré Interferometry Displacement Fields. *Experimental Mechanics*, 53(4), 635–648. ISSN 0014-4851, 1741-2765. doi:10.1007/s11340-012-9671-8.

[4] Sepahvand, K. and Marburg, S. (2015). Non-sampling inverse stochastic numerical–experimental identification of random elastic material parameters in composite plates. *Mechanical Systems and Signal Processing*, 54-55, 172–181. ISSN 08883270. doi: 10.1016/j.ymssp.2014.09.011.

[5] Uhart, M., Patrouix, O., and Aoustin, Y. (2014). Improving accuracy in robotized fibre placement using force and visual servoing external hybrid control scheme. 44 pages, soumis au journal ROBOTICA.

[6] Scarth, C., Cooper, J. E., Weaver, P. M., et al. (2014). Uncertainty quantification of aeroelastic stability of composite plate wings using lamination parameters. *Composite Structures*, 116, 84–93. ISSN 02638223. doi:10.1016/j.compstruct.2014.05.007.

[7] Verchery, G. (1979). Les invariants des tenseurs d'ordre 4 du type de l'élasticité. vol. 115. Villard-de-Lans: Éditions du CNRS, Paris, pp. 93–104.

[8] Reddy, J. N. (1999). *Theory and analysis of elastic plates*. Philadelphia, PA: Taylor & Francis. ISBN 1560327057 9781560327059.

[9] Stodieck, O., Cooper, J. E., Weaver, P. M., et al. (2013). Improved aeroelastic tailoring using tow-steered composites. *Composite Structures*, 106, 703–715. ISSN 02638223. doi:10.1016/j.compstruct.2013.07.023.

[10] Wright, J. R. and Cooper, J. E. (2015). *Introduction to aircraft aeroelasticity and loads*. Chichester: Wiley, 2. ed ed. ISBN 9781118488010 9781118488010 9781118700426.

[11] Soize, C. and Ghanem, R. (2004). Physical Systems with Random Uncertainties: Chaos Representations with Arbitrary Probability Measure. *SIAM Journal on Scientific Computing*, 26(2), 395–410. ISSN 1064-8275, 1095-7197. doi:10.1137/S1064827503424505.

[12] Navarro Jimenez, M.I., Witteveen, J.A.S., and Blom, J.G. (2014). Polynomial Chaos Expansion for general multivariate distributions with correlated variables. Tech. rep., Centrum Wiskunde & Informatica.

[13] Vannucci, P. (2005). Plane Anisotropy by the Polar Method*. *Meccanica*, 40(4-6), 437–454. ISSN 0025-6455, 1572-9648. doi:10.1007/s11012-005-2132-z.

[14] Julien, C. (2010). *Conception Optimale de l'Anisotropie dans les Structures Stratifiées à Rigidité Variable par la Méthode Polaire-Génétique*. Ph.D. thesis, Sorbonne Universités, Université Pierre et Marie Curie Paris 6/CNRS, UMR 7190, Paris.

[15] Wan, X. and Karniadakis, G. E. (2006). Beyond Wiener–Askey Expansions: Handling Arbitrary PDFs. *Journal of Scientific Computing*, 27(1-3), 455–464. ISSN 0885-7474, 1573-7691. doi:10.1007/s10915-005-9038-8.

[16] Mathelin, L., Hussaini, M. Y., and Zang, T. A. (2005). Stochastic approaches to uncertainty quantification in CFD simulations. *Numerical Algorithms*, 38(1-3), 209–236. ISSN 1017-1398, 1572-9265. doi:10.1007/BF02810624.